Applied Thermal Engineering 93 (2016) 139–146

Contents lists available at ScienceDirect

Applied Thermal Engineering

journal homepage: www.elsevier.com/locate/apthermeng

Research Paper

Experimental studies on a novel thin flat heat pipe heat spreader

Ji Li [a,*], Lucang Lv [b]

[a] Laboratory of Advanced Thermal Management Technologies, College of Physics, University of Chinese Academy of Sciences, 19A Yu-quan-lu Road, Shijingshan District, Beijing 100049, China

[b] College of Physics, University of Chinese Academy of Sciences, 19A Yu-quan-lu Road, Shijingshan District, Beijing 100049, China

HIGHLIGHTS

- A thin flat heat pipe with novel wick structure was fabricated.
- Operation characteristics of the flat heat pipe were identified.
- High heat flux of 100 W/cm² was achieved for this 2 mm flat heat pipe.
- Gravity has very small impact on its thermal performance.

ARTICLE INFO

Article history:
Received 31 May 2015
Accepted 15 September 2015
Available online

Keywords:
Flat heat pipe
Thermal performance
Wick structure
Electronics cooling

ABSTRACT

The thermal performance of a copper-water flat heat pipe (100 mm × 50 mm × 2 mm) composed of a novel wick structure with an inner thickness for working fluid less than 1 mm has been investigated. The wick structure was made of sintered hybrid copper fine powder with diameters ranging from 50 µm to 100 µm. The effects of heating input, tilt angle, and cooling temperature on flat heat pipe working performance were studied experimentally. Results showed that the proposed flat heat pipe could effectively dissipate 120 W (100 W/cm²) in the horizontal orientation with a thermal resistance of 0.196 °C/W. Moreover, it has been demonstrated that under air natural convection condition, the performances of the novel flat heat pipe were higher than those of thin copper sheet, showing an effective thermal conductivity more than 4 times of copper.

1. Introduction

The heat per unit area generated by chips continuously increases and thermal control becomes a very attractive research topic in the electronic industry. Local and global high temperatures can both significantly influence the working performance of the electronic components or lead to high thermal stress [1]. Thus, to cool these devices efficiently in narrow spaces, thin, high-performance, and lightweight cooling devices are demanded. Micro/mini flat heat pipe is one of the most promising approaches for the thermal management of electronic components [2], especially for high power mobile electronics, e.g., portable game PC or automobile LED lighting.

The early information concerning the micro/mini-scale heat pipes can be found in [3]. In the past two decades, many investigations on the working performance of thin flat heat pipes have been carried out. One of the most common wick structures is micro/mini grooves [4–7]. Cao et al. [4] tested a 2 mm-thick rectangular-grooved heat pipe which had a maximum heat transfer rate of 24.8 W when cooled at 90 °C. Hopkins et al. [5] experimentally investigated a 2.4 mm-thick flat heat pipe with micro trapezoidal capillary grooves manufactured by a rolling method. When heated at both sides of the evaporation section and positioned in the horizontal orientation, the flat heat pipe had a minimum thermal resistance of 0.3 °C/W with a maximum heat flux of 17.3 W/cm². Lin et al. [8] made a 6.35 mm thick flat heat pipe whose wick structure was a folded copper sheet fin. A maximum heat flux of 158 W/cm² (122.3 W) was obtained when the evaporator temperature reached 112.6 °C. In 2008, Lim et al. [9] presented a relatively small flat copper heat pipe (56 mm × 8 mm × 1.5 mm) with radial microgrooves fabricated by using a femtosecond laser micromachining technique. This device could only perform functionally at heat loads below 12 W cooled by a refrigeration bath circulator. Recently, Zaghdoudi et al. [6] found that the thermal resistance of flat heat pipe decreased with the increase of the heat sink temperature.

By flattening a metal tube, some flat heat pipes [10–12] have been fabricated. The limitation for the pressed thickness between 2 mm and 2.5 mm was obtained by Moon et al. [10]. With sintered copper powder wick structure, the spreading resistance from the heat source to the evaporator for a 5 mm thick flat heat pipe [13] was measured about 40 times smaller than that of the copper plate at 28 W/cm². Rulliere et al. [14] studied the maximum heat transfer capability of a flat heat pipe with a large evaporator area. A small thermal

* Corresponding author. Tel.: +86 13522278866; Fax: +86-010-69671698.
E-mail address: jili@ucas.ac.cn (J. Li).

http://dx.doi.org/10.1016/j.applthermaleng.2015.09.038
1359-4311/

resistance of 0.05 °C/W was obtained at 155 W. Tsai et al. [15] tested a copper-water vapor chamber with an inner height of 1.4 mm and its maximum heat transfer rate was 50 W. Some wire mini-heat pipes [16,17] were also investigated experimentally. To sum up, the above-mentioned researches showed that the different types of metal thin flat heat pipes could only work functionally under relatively low heat fluxes when the inner height was less than 1.5 mm and the saturation temperature was within 60 °C.

To further decrease the thickness, some researchers [18–21] studied the behavior of silicon-based flat heat pipes with microscale capillary grooves. Moreover, Ding et al. [22] presented a Ti-based flat heat pipe (30 mm × 30 mm × 0.6 mm) that could dissipate 7.2 W. Oshman et al. [23–25] fabricated three different polymer-based flat heat pipes whose inner heights were 1 mm [23], 1 mm [24], and 0.9 mm [25], respectively. The performance of the heat pipe [23] with a hybrid wick structure consisting of micro pillars and woven mesh was tested; experimental results showed that the heat pipe could work under 11.94 W at adverse-gravity direction. Famouri et al. [26] numerically investigated the transient heat transfer in this flat heat pipe. However, the application of these silicon/polymer-based flat heat pipes will be confined in consideration of their reliability and fabrication.

With the assistance of visualization, Wong [27,28], Lefevre and their staffs [29–31] studied the thermal performance and the mechanism inside flat heat pipes with small internal space. As declared in [29], the presence of nucleate boiling could improve the thermal performance of a flat heat pipe; moreover, the heat flux at the beginning of the nucleate boiling was much lower than the dry-out heat flux. With n-pentane as the working fluid, the effect of the vapor space thickness on the thermal performance of a flat heat pipe has been analyzed systematically in [30].

The above-mentioned researches highlight that the limited spaces available for the evaporation process and for the fluid circulation limit the high performance of flat heat pipes. In particular, thickness plays a key role in flat heat pipe performances. Meanwhile, the above-referred works all adopted traditional structure, as being used in a conventional heat pipe or a conventional vapor chamber, in which vapor phase and liquid phase flow reversely inside the envelope, especially at the evaporation zone.

The present work describes a thin high-performance copper-water flat heat pipe in detail, aiming to cool high power portable electronics or optoelectronic equipment. This flat heat pipe has a novel sintered hybrid copper powder wick structure, whose internal space height is less than 1 mm. The working performance of the heat pipe device has been tested and analyzed under different heat loads, tilt angles, and cooling water temperatures. Furthermore, the thermal performance of the flat heat pipe device under natural convection at different heating inputs has been evaluated both experimentally and numerically. In addition, a comparison has been made using a copper plate with the same size of the proposed device. Experimental tests demonstrated that this flat heat pipe could manage high heat flux with a quite low thermal resistance.

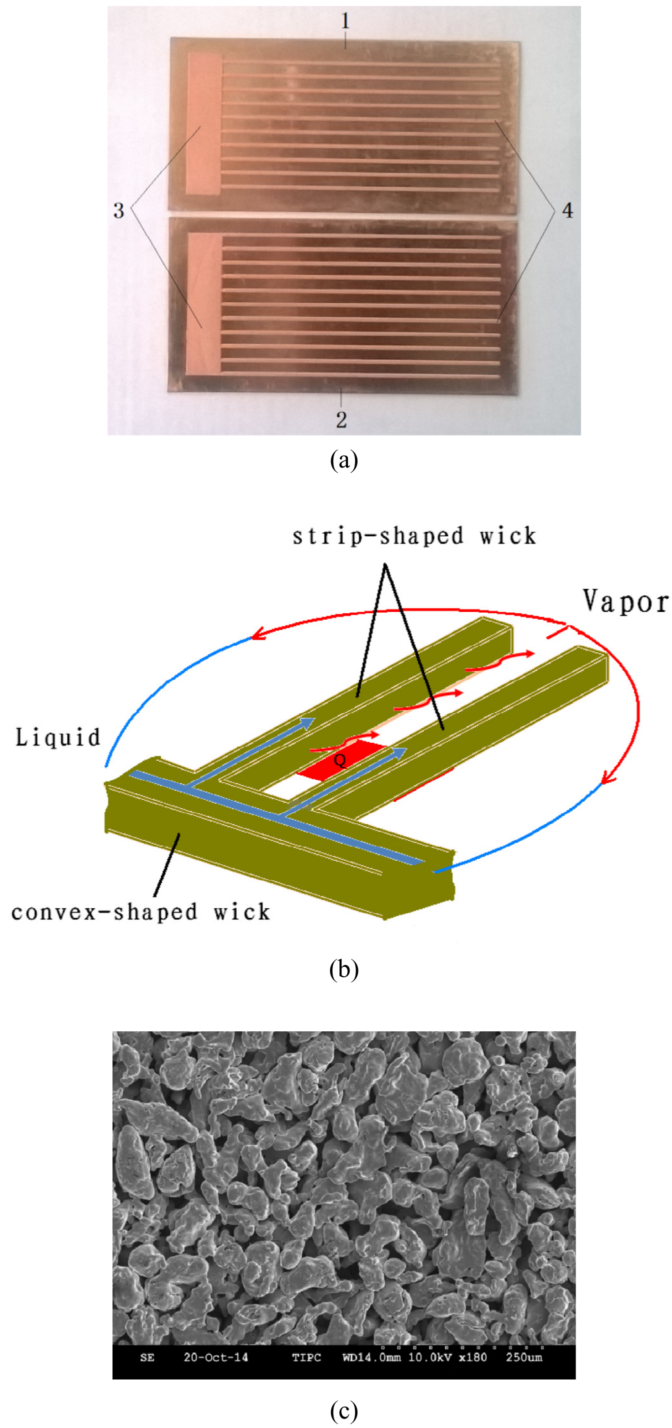

Fig. 1. Flat heat pipe schematic: (a) upper and lower plates; (b) working mechanism; (c) sintered hybrid powder wick.

2. Heat pipe construction

The proposed flat heat pipe is primarily composed of two copper plates with sintered wick structure on the inner surface. Referring to Fig. 1a, 1 and 2 are the copper plates, 3 and 4 are sintered copper powder wick structures; the convex region collects condensate, while liquid flows within the striped region. Both convex and striped regions also serve as the supporting structure to avoid concave deformation during the fabrication and operation process. The channels formed by the strip-shaped wick structures are the paths for the vapor and part of the returned liquid. This type of sintered wick structures is believed to enhance the working efficiency of flat heat pipe by lowering the thermal resistance, because the flow of most part of liquid and vapor is restricted mainly in the same direction. Therefore, the flow resistance is reduced by restraining the counterflow as happening in conventional heat pipes, which is somewhat similar to the working mechanism of loop heat pipe described in [32]. Fig. 1b shows the flow inside the flat heat pipe schematically. The vapor generated in the wicked strips near the convex region flows through the channels formed between the wicked strips and the condensate returns driven by capillary force and accumulates in the convex region. Meanwhile, in order to provide a high capillary force and a low flow resistance in the wick, hybrid copper

Table 1
Main geometrical parameters (in mm).

Overall dimensions of the flat heat pipe (L × W × H)	100 × 50 × 2
Overall dimensions of the copper casing (L × W × H)	100 × 50 × 0.5
Dimensions of the convex-shaped wick (L × W × H)	41 × 10 × 0.5
Dimensions of single strip-shaped wick (L × W × H)	80 × 1 × 1
Number of the strip-shaped wick	21
Number of the vapor channels	22

powder with different size (300 mesh powder and 30% in weight, and 150 mesh powder and 70% in weight) was mixed and sintered together, as shown in Fig. 1c. Table 1 summarizes the main geometrical parameters of the proposed flat heat pipe.

In order to enhance the mechanical strength and reliability of the flat heat pipe, the two copper plates have been aligned and fixed together through a secondary sintering process. Any possible gap between the copper plate and the wick structure is removed through secondary sintering process; therefore, the heating source can be mounted on any one of the two surfaces of the flat heat pipe without any negative effects on the thermal performance. Water was chosen as the working fluid, and following an evacuation process ($<5 \times 10^{-3}$ Pa), a charging ratio of 45% was selected through extensive preliminary experiments aiming to reach a compromise between the preferred thermal resistance and the possible maximum heat load. Here, the charging ratio is defined as the volume percentage of the total inner space of the flat heat pipe including the porosity of the wick shared by the working fluid. Fig. 2 shows the final heat pipe after welding and charging processes.

3. Experimental setup

Fig. 3 illustrates the experimental testing system. A DC power supplier provides electrical power to a copper block containing a cartridge heater as the heating source, as presented in Fig. 4a. The heating block is mounted at the upper surface of the flat heat pipe, whose active heating area is 12 mm ×10 mm. To minimize the environmental heat losses, the heating copper block and the adiabatic section of the heat pipe are wrapped with a layer of 10 mm-thick adiabatic foam made of NBR/PVC (Fig. 4b); its thermal conductivity is 0.04 W/(m·°C). In addition, a very thin layer of thermal grease (conductivity about 6 W/(m·°C)) fills the gap between the heat pipe and the copper heating block to minimize the contact thermal resistance. A water cooling chamber (50 mm × 50 mm) screwed to the heat pipe cools it. The cooling water flow rate is set as 4 L/min and a thermostatic water bath (DC-2020) controls its inlet temperature.

An Agilent 34970A data acquisition system monitors and records the temperatures acquired by eleven T-type Omega thermocouples firmly attached to the surface of the flat heat pipe. Sampling duration is 3 s and thermocouple accuracy is ±0.5 °C. Fig. 5 shows the position of the microscale thermocouples on heat pipe surface. The temperatures from 103 to 107, discussed in the following sections, are the averaged values, e.g., the temperature (103) is the mean value of temperatures at the locations of 103_1 and 103_2. To make sure that thermocouples correctly adhere to the flat heat pipe, before each test the electro-conductance between the thermocouples and the flat heat pipe was measured. Thermocouple 101 shown in Fig. 4 monitors the central temperature at the top surface of the heating block. Another thermocouple (113), as shown in Figs. 3 and 4b, was attached to the surface of the thermal insulation wrapping the heating block to evaluate the heating losses from the insulating layer surface to the ambient. Considering natural convection and thermal radiation, this heat loss never exceeded the 3.5% of the heating power in all testing cases.

Fig. 2. Prototype of a flat heat pipe.

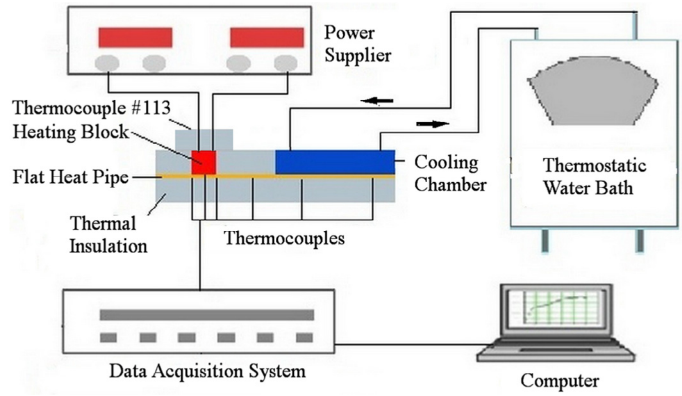

Fig. 3. Schematic of the experimental setup.

4. Working performance evaluation

The thermal resistance and the operation temperature are commonly used to evaluate the working performance of a heat pipe. In this paper, the total thermal resistance of the tested prototype and the thermal resistance of the flat heat pipe are calculated by Eq. (1) and Eq. (2), respectively.

$$R_{system} = \frac{T_{case} - T_{coolant}}{Q} \tag{1}$$

$$R_{HP} = \frac{T_e - T_c}{Q} \tag{2}$$

Here Q is the heating input power provided by the DC supplier; T_{case} and $T_{coolant}$ are the temperature at the top surface center of the heating block (T_{101}) and the inlet temperature of the cooling water, respectively. T_e is the evaporation temperature measured by the thermocouple 102; T_c is the condensation temperature calculated by averaging the temperatures measured by four thermocouples (106_1, 106_2, 107_1, and 107_2).

Under a cooling water temperature of 35 °C and in the horizontal direction, the uncertainties of R_{HP} and R_{system} were calculated as 2.14~5.26% and 2.19~5.25%, respectively, through the synthetic method for relative error analysis by Eq. (3).

$$\frac{\delta R}{R} = \sqrt{\left(\frac{\delta Q}{Q}\right)^2 + \left[\frac{\delta(T_e - T_c)}{T_e - T_c}\right]^2} \tag{3}$$

4.1. Comparison between flat heat pipe and copper plate

The temperature of water flowing through the cooling chamber was initially set as 35 °C. Figs. 6 and 7 plot the steady state temperatures at different locations on the flat heat pipe and the copper

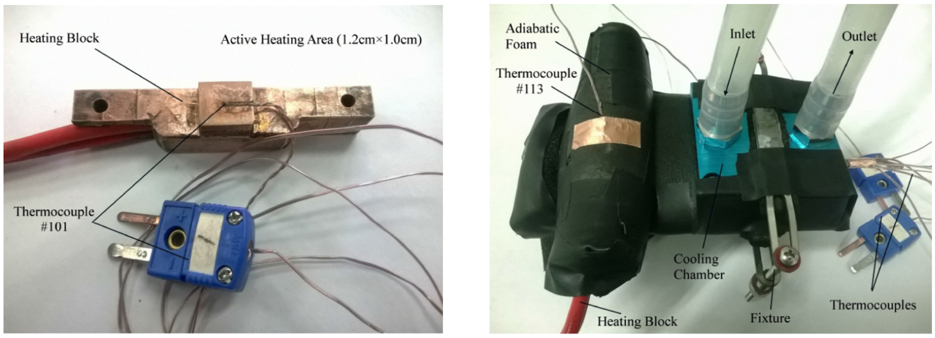

(a) (b)

Fig. 4. Configuration of the testing: (a) structure of the heating block; (b) assembling.

plate is positioned horizontally respectively. Plots highlight that temperatures of the flat heat pipe were lower than those of the copper plate in all tested conditions, and the difference increased with the heat load increasing. For the thermocouples 101 and 102, at 120 W, the temperature differences were 83.8 °C and 99.4 °C, respectively. Moreover, the temperature difference between the heated and the cooled sections of the copper plate was much higher than that of the flat heat pipe for all heat loads, and the values increased greatly with the increase of heating input. For example, the temperature difference of the flat heat pipe was 20.8 °C while that of the copper plate was 111.3 °C at 108 W, nearly 5.4 times larger than the heat pipe. In addition, due to the excess of water flooding at the end of condenser, the temperature at location of 107 grew a little with the heat load increasing. This phenomenon might be also explained considering the possible presence of small amount of non-condensable gas, which prevented the vapor from spreading to the end of condenser. In consideration of these negative factors, the temperature of the proposed flat heat pipe is still uniform compared with that of the copper plate; for the flat heat pipe, there is a very small temperature difference among the measuring points 103, 104 and 105.

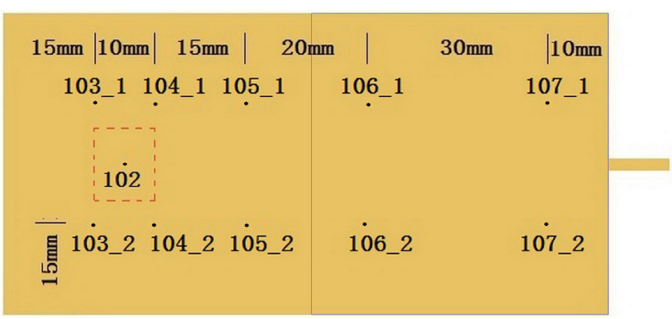

Fig. 5. Locations of the thermocouples (the red dash square represents the heater position). (For interpretation of the references to color in this figure legend, the reader is referred to the web version of this article.)

Fig. 8 shows the thermal resistances of both the flat heat pipe and the copper plate under different heating inputs. The thermal resistances of the test system and of the heat pipe itself decreased rapidly initially and then slowed down with the increase of the heat load. The measured corresponding thermal resistances were 0.490 °C/W and 0.193 °C/W at 108 W, respectively. Then, thermal resistance slightly increased at 120 W. In addition, the proportion in the total thermal resistance of the testing system taken by the flat heat pipe decreased with the heating input increasing below 108 W. With regard to the copper plate system and the copper plate, all studied cases almost showed the same thermal resistances (approximately 1.20 °C/W and 1.04 °C/W, respectively).

At relatively low heat loadings, the evaporation process is not very intensive and the water film in the evaporator is relatively thick, directly leading to a large thermal resistance of the evaporation section. As the heating input increases, the water film became thin.

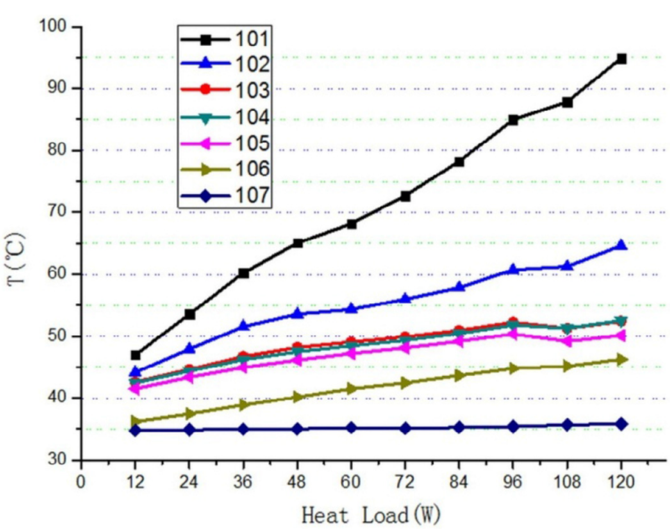

Fig. 6. Temperatures at different locations on the flat heat pipe.

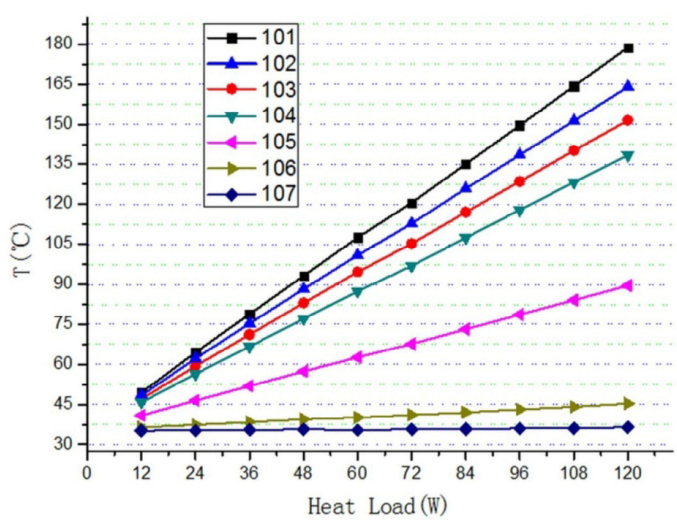

Fig. 7. Temperatures at different locations on the copper plate.

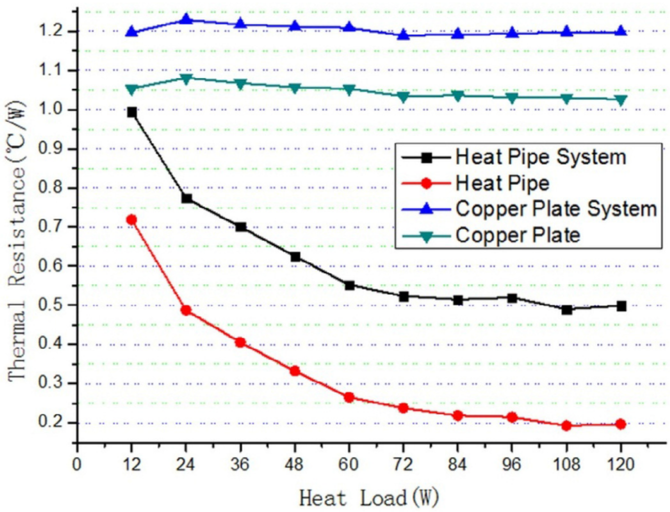

Fig. 8. Thermal resistance under different heat loads.

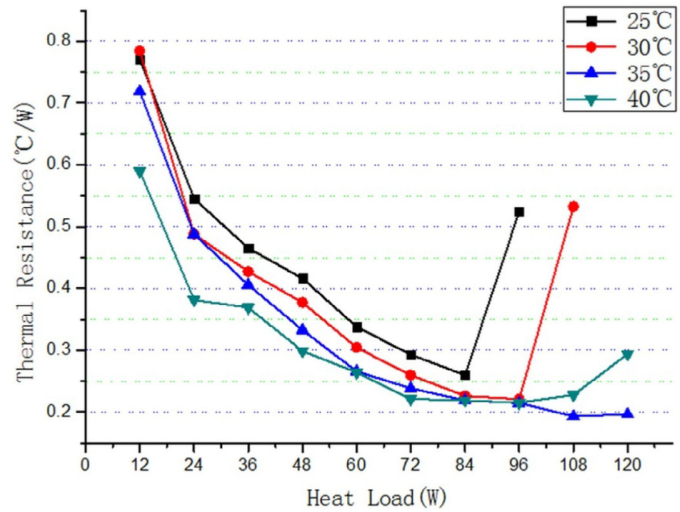

Fig. 9. Flat heat pipe thermal resistances under different cooling water temperatures.

Moreover, the difference of the meniscus radius of the liquid–vapor interface between the evaporator and the condenser increases and the velocities of the vapor and the liquid both increase, accelerating the heat transfer in flat heat pipe. As a result, the thermal resistance of flat heat pipe will decrease. When the heat load reaches up to the value at which the capillary cannot balance the flow resistance, it is assumed that the water film will become very thin and a partial dry-out will take place. Thus, the evaporator temperature will increase in turn and thermal resistance will increase.

Table 2 shows the comparison of the heat transfer capability of various flat heat pipe designs in the horizontal orientation. Results show that the working performance of the proposed flat heat pipe in this work is better than other reported flat heat pipes in terms of dimensions and overall performance, thanks to the novel wick structure. The comparison indicates that the unique wick structure coupled with the hybrid porous size allows reducing the thickness of metal flat heat pipes without significant deterioration in performances.

4.2. *Effect of cooling water temperature*

The effect of cooling water temperature on thermal performance of the flat heat pipe in the horizontal orientation has been investigated. The thermal resistances of the flat heat pipe for different study cases are plotted in Fig. 9. It can be seen that the thermal resistance decreased with the cooling water temperature increasing before dry-out occurring. As explained in [31], the increase of cooling water temperature leads to the decrease of vapor and liquid friction factor which directly decreases the vapor pressure drop and the liquid pressure drop.

The minimum thermal resistances for 25 °C, 30 °C, 35 °C and 40 °C were 0.260 °C/W (84 W), 0.221 °C/W (96 W), 0.193 °C/W (108 W) and 0.215 °C/W (96 W), respectively. The comparison among the thermal resistance curves indicates that the lowest value at high heat loads exists when the cooling water is 35 °C, meaning that there exists an optimal water cooling temperature for a special flat heat pipe.

Table 2
Performance comparison of various typical flat plate heat pipe designs.

References	Material, temperature (°C)	Inner height (mm)	Heat flux (W/cm^2)/ heat load (W)	Thermal resistance (°C/W)
Launay et al. [18]	Silicon/ethanol, $T_{coolant} = 30$	0.17	3/3	≈3
Ding et al. [22]	Ti/water, –	0.2	7.2/7.2	2.69
Launay et al. [18]	Silicon/methanol, $T_{coolant} = 30$	0.342	2/2	0.8
Ivanova et al. [19]	Silicon/water, $T_{coolant} = 50$	0.47	70/70	0.9
Zaghdoudi et al. [6]	Copper/water, $T_{coolant} = 40$	0.5	4.2/40	≈0.72
Yang et al. [21]	Silicon/water, –	0.6	7.35/18	1.32
Cao et al. [4]	Copper/water, $T_{coolant} = 90$	0.8	14/31	≈0.6
Oshman et al. [25]	Polymer/water, $T_{coolant} = 10$	0.9	2.88/18	1.2
Cao et al. [4]	Copper/water, $T_{coolant} = 90$	1	20.6/24.8	≈0.8
Oshman et al. [24]	Polymer/water, $T_{coolant} = 10$	1	62.5/40	0.25
Oshman et al. [23]	Polymer/water, –	1	11.94/11.94	≈1.1
Present work	**Copper/water, $T_{coolant} = 35$**	**1**	**100/120**	**0.196**
Lim et al. [9]	Copper/water, –	1.1	12/12	≈5.1
de Paiva et al. [17]	Copper/water, $T_v = 56$	1.4	7.5/45	≈0.4
Tsai et al. [15]	Copper/water, $T_{coolant} = 40$	1.4	44.2/50	0.868
Hopkins et al. [5]	Copper/water, $T_v = 90$	1.51	11/16	0.5
Chen and Chou [7]	Aluminum/acetone, $T_{coolant} = 25$	1.7	3.13/47	0.254
Hopkins et al. [5]	Copper/water, $T_v = 90$	1.9	17.3/22	0.3
Rulliere et al. [14]	Copper/methanol, $T_v = 70$	1.98	0.9/155	0.05
Lips et al. [30]	Copper/water, $T_v = 40$	2	10/140	0.24
Wang and Peterson [16]	Copper/water, $T_v = 85$	2	19.1/123	–

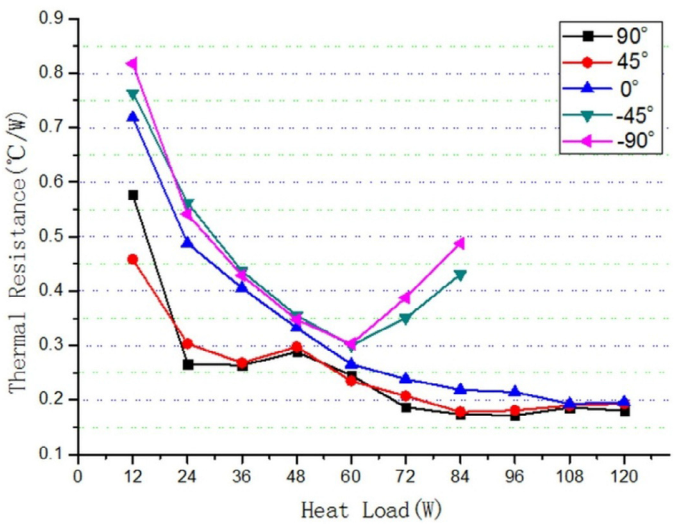

Fig. 10. Thermal resistance of the flat heat pipe under different tilt angles.

4.3. *Effect of tilt angle*

To investigate the effect of gravity on the thermal performance, the flat heat pipe was tested under different tilt angles (–90°, –45°, 0°, 45° and 90°) setting the cooling water temperature at 35 °C. The thermal resistances of the flat heat pipe with varying tilt angles and heat loads are presented in Fig. 10. When the evaporation zone was laid above the condensation zone (negative tilt angles), the condenser was partially full of liquid-phase working fluid. The unbalanced capillary and gravity forces could not keep the working fluid circulating in the flat heat pipe at high heat loads, and the minimum thermal resistance of 0.303 °C/W was obtained at 60 W. When the evaporation section was at the bottom end (positive tilt angles), it was filled with liquid-phase working fluid. The capillary force and the gravity force worked together to maintain the flat heat pipe operating. At 96 W, the minimum thermal resistances were 0.180 °C/W and 0.172 °C/W, respectively, for 45° and 90° tilt angles.

Moreover, the thermal resistances were almost the same for –45° and –90° tilt angles at a given heating load, meaning that the working performances of the flat heat pipe are almost the same. The same behavior could be observed for positive tilt angles. For 0° tilt angle and heat loads not exceeding 60 W, the thermal performance of the flat heat pipe was similar to that in the negative orientation; at relatively high heating inputs (more than 60 W), the evaporator temperature and the thermal resistance roughly showed the same changing trend as that for positive tilt angles. In general, due to the high capillary force and low flow resistance provided by the fine hybrid powder coupled with a relatively high filling ratio of working liquid, the performance of the flat heat pipe at horizontal position lies between the negative and positive positions.

5. Performance assessment under air natural convection

The thermal performance of the flat heat pipe in the horizontal orientation has been evaluated under air natural convection condition for portable electronics applications. A 10 mm × 10 mm ceramic heater was attached to the upper surface of the flat heat pipe by using a layer of 0.1 mm-thick double-faced adhesive tape with a thermal conductivity of 1.5 W/(m·°C). The external surface of the flat heat pipe was entirely exposed to air. For all heating inputs, the ambient temperature value was kept at 25 ± 1.3 °C and the heat loss by natural convection and thermal radiation from the heater surface to the ambient did not exceed 5%. The effective thermal conductivity is calculated by Eq. (4):

$$k_{eff} = Q' \cdot \frac{L_{eff}}{A\Delta T} \tag{4a}$$

$$Q' = \frac{L_{eff}}{L} Q, \tag{4b}$$

where Q is the heating input power; L_{eff} is the distance between the center of the evaporator and the location of the thermocouple farthest from the evaporator. L and A are the total length and the cross section area of the flat heat pipe, respectively; ΔT represents the temperature difference along the L_{eff}. It should be noted that Eq. (4b) calculates the portion of the heat load dissipated from the surface where the thermocouples are located. Fig. 11 plots the calculated effective thermal conductivities of copper plate and of heat pipe. Since Eq. (4) calculates roughly the effective thermal conductivity of a heat pipe heat spreader, a 3D heat conduction model has been established to validate the formula in this work and results are also plotted in Fig. 11 (referring to the Appendix for the detailed 3D model). Plotting shows that the effective thermal conductivity of the flat heat pipe increased with the increase of the heating input, reaching a maximum value of 1617 W/(m·°C) at the maximum heat load of 8.80 W. The effective thermal conductivity of the copper plate was almost the same for different testing cases.

The error of copper effective thermal conductivities (known as conductivity, 380 W/(m·°C)) calculated by Eq. (4) compared to the 3D model is less than 10%. This difference depends on two main factors: the uncertainty of the actual heat load and the influence of the spanwise heat conduction. However, Eq. (4) gives a simple and straight approach to calculate the effective conductivity with measured data.

Fig. 12 shows the comparison of the temperature distributions on the external surface of the heat pipe and that of copper sheet opposite to the heating side. For both cases, the comparisons between the 3D simulations and the infrared measurements are shown. The difference of the measured and simulated temperature magnitude is less than 1 °C for both cases. In summary, the novel flat heat pipe has a much more even temperature distribution than copper and the highest temperature in heat pipe is quite lower than copper

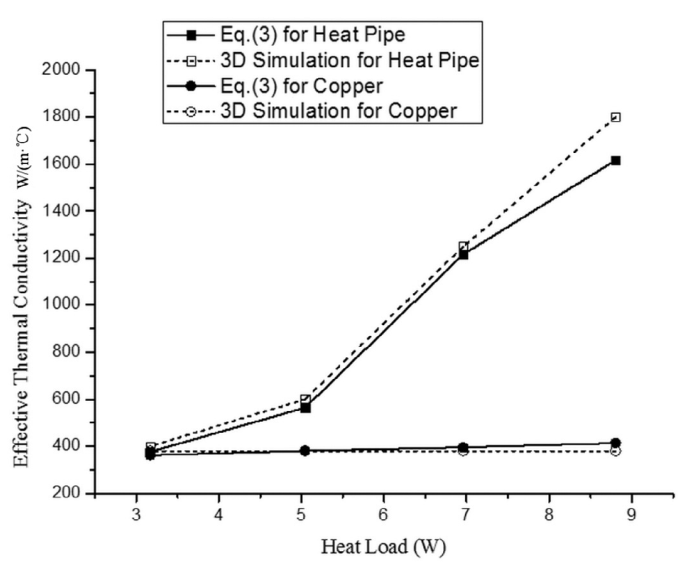

Fig. 11. Effective thermal conductivity under different heat loads.

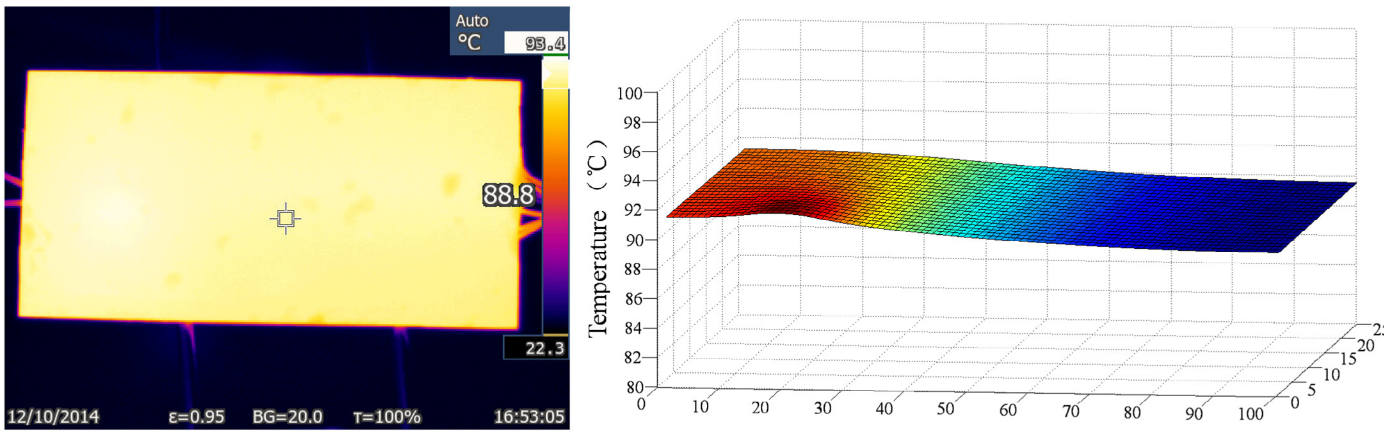

(a) Heat pipe

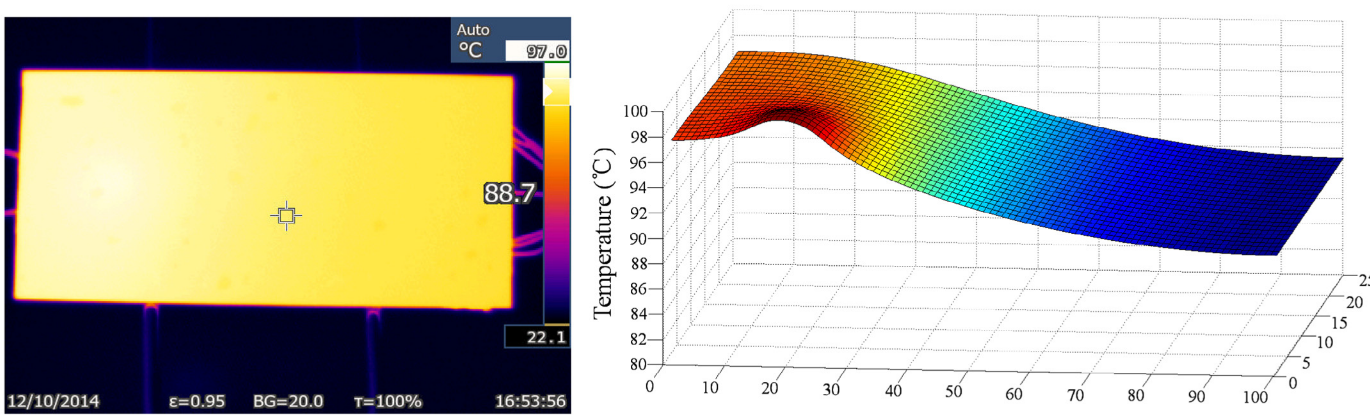

(b) Copper

Fig. 12. Comparisons of temperature distributions at 8.80 W: (a) heat pipe; (b) copper.

under the same heat load (e.g., about 8 °C at 8.8 W measured at the heating side).

6. Conclusions

A copper-water flat heat pipe composed of a novel wick structure has been fabricated and investigated. Its working performance has been evaluated under different heat loads, cooling water temperatures, and tilt angles. Experimental results indicate that the heat pipe could effectively dissipate 120 W (~100 W/cm^2) in the horizontal orientation. And a minimum thermal resistance of 0.196 °C/W was measured at 108 W, less than one fifth of that of the copper plate with the same dimension. Tests qualitatively showed that there exists an optimal cooling water temperature at which the flat heat pipe reaches its best performance.

Furthermore, the proposed flat heat pipe has much better performance than thin copper sheet under air natural convection condition for portable electronics cooling, reaching an effective thermal conductivity more than 4 times of copper.

Acknowledgements

This work is supported by the National Natural Science Foundation of China (Project No. 51176202).

Appendix

The 3D heat conduction model used in this investigation about the heat spreading in the heat pipe or copper sheet is presented here in detail. As shown in Fig. A1, a three-dimensional steady-state heat conduction model was used for the present study.

$$\frac{\partial}{\partial x}\left(\lambda\frac{\partial T}{\partial x}\right)+\frac{\partial}{\partial y}\left(\lambda\frac{\partial T}{\partial y}\right)+\frac{\partial}{\partial z}\left(\lambda\frac{\partial T}{\partial z}\right)=0 \qquad \text{(a-1)}$$

This equation is subjected to the following thermal boundary conditions (refer to Fig. A1):

$$z=0,\quad 0.015\le y\le 0.025,\quad \text{and}\quad -0.005\le x\le 0.005,\quad -\lambda\frac{\partial T}{\partial x}=q \qquad \text{(a-2a)}$$

$$\text{on the other surfaces,}\quad -\lambda\frac{\partial T}{\partial x}=\alpha(T-T_0)+\varepsilon\sigma\left(T^4-T_0^4\right) \qquad \text{(a-2b)}$$

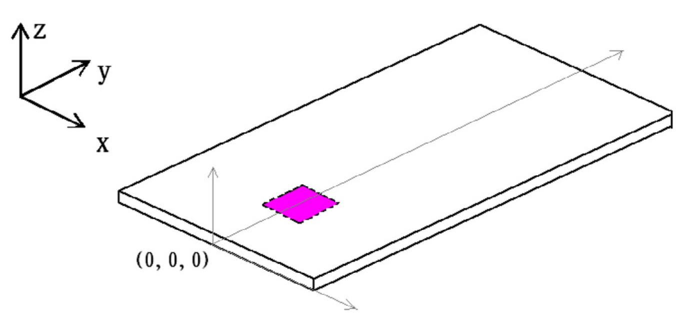

Fig. A1. 3D heat conduction modeling.

where $q = \frac{Q}{A} = \frac{Q}{1\times10^{-4}}$; the emissivity of the surface was chosen as 0.45 for the oxidized copper and 0.95 for the black paint (here we pasted a black paint on the external surface of the tested articles for IR photography and the emissivity was set by referring to the textbook [33] and using a one-dimensional thermal balance analysis); σ is the Stefan–Boltzmann constant $\sigma = 5.669 \times 10^{-8}$ W/m^2·K^4. Here, the conductivity λ will be determined from matching the temperature distributions with the measured data.

Equation (a-2a) yields the third boundary condition, and the natural convection heat transfer coefficient α is adopted from the well-accepted correlations proposed by W. H. McAdams [34] for fluid natural convection on a horizontal heated surface:

$$\text{on the upper side,} \quad Nu = 0.54 Ra_f^{0.25} \tag{a-3a}$$

$$\text{on the bottom side,} \quad Nu = 0.27 Ra_f^{0.25} \tag{a-3b}$$

where Ra_f is the Raleigh number, $Ra_f = Gr_f \cdot \Pr$, and Gr_f is the Grashof number,

$$Gr_f = \frac{\beta \cdot \Delta T \cdot g \cdot (L)^3}{\upsilon_f^2} \tag{a-4}$$

L is the characteristic length of the domain (here L = 100 mm), $\beta = 1/T$, $g = 9.8$, $\Delta T = T - T_0$, and υ_f is the kinetic viscosity of the fluid.

Nomenclature

A	Cross-section area, m^2
g	Acceleration of gravity
L	Length, m
k	Effective thermal conductivity, W/(m·°C)
q	Heat flux, W/m^2
Q	Heating load, W
R	Thermal resistance, °C/W
T	Temperature, °C
α	Heat transfer coefficient, W/(m^2·°C)
β	Volume coefficient of expansion, 1/K
ε	Emissivity
λ	Thermal conductivity, W/(m·°C)
υ	Kinetic viscosity, m^2/s

Subscript

e	Evaporation
c	Condensation
v	Vapor

References

[1] P.H. Chen, S.W. Chang, K.F. Chiang, J. Li, High power electronic component: review, Recent Pat. Eng. 2 (2008) 174–188.
[2] L.C. Lv, J. Li, Micro flat heat pipes for microelectronics cooling: review, Recent Pat. Mech. Eng. 6 (2013) 169–184.
[3] G.P. Peterson, An Introduction to Heat Pipes, Wiley, New York, 1994.
[4] Y. Cao, M. Gao, J.E. Beam, B. Donovan, Experiments and analyses of flat miniature heat pipes, J. Thermophys. Heat Transfer 11 (1997) 158–164.
[5] R. Hopkins, A. Faghri, D. Khrustalev, Flat miniature heat pipes with micro capillary grooves, J. Heat Transfer 121 (1999) 102–209.
[6] M.C. Zaghdoudi, S. Maalej, J. Mansouri, M.B.H. Sassi, Flat miniature heat pipes for electronics cooling: state of the art, experimental and theoretical analysis, World Acad. Sci. Eng. Technol. 51 (2011) 879–902.
[7] J.S. Chen, J.H. Chou, Cooling performance of flat heat pipes with different liquid filling ratios, Int. J. Heat Mass Transfe. 77 (2014) 874–882.
[8] L. Lin, R. Ponnappan, J. Leland, High performance miniature heat pipe, Int. J. Heat Mass Transfe. 45 (2002) 3131–3142.
[9] H.T. Lim, S.H. Kim, H.D. Im, et al., Fabrication and evaluation of a copper flat micro heat pipe working under adverse-gravity orientation, J. Micromech. Microeng. 18 (2008) 105013.
[10] S.H. Moon, G. Hwang, H.G. Yun, et al., Improving thermal performance of miniature heat pipe for notebook PC cooling, Microelectron. Reliabil. 42 (2002) 135–140.
[11] S.F. Wang, J. Chen, Y. Hu, W. Zhang, Effect of evaporation section and condensation section length on thermal performance of flat plate heat pipe, Appl. Therm. Eng. 31 (2011) 2367–2373.
[12] M.H.A. Elnaggar, M.Z. Abduuah, S.R.R. Munusamy, Experimental and numerical studies of finned L-shape heat pipe for notebook-PC cooling, IEEE Trans. Components Packaging Manuf. Technol. 3 (2013) 978–988.
[13] R. Boukhanouf, A. Haddad, M.T. North, C. Buffone, Experimental investigation of a flat heat pipe performance using IR thermal imaging camera, Appl. Therm. Eng. 26 (2006) 2148–2156.
[14] R. Rulliere, F. Lefevre, M. Lallemand, Prediction of the maximum heat transfer capability of two-phase heat spreader – experimental validation, Int. J. Heat Mass Transfe. 50 (2007) 1255–1262.
[15] M.C. Tsai, S.W. Kang, K.V. de Paiva, Experimental studies of thermal resistance in a vapor chamber heat spreader, Appl. Therm. Eng. 56 (2013) 38–44.
[16] Y. Wang, G.P. Peterson, Investigation of a novel flat heat pipe, J. Heat Transfer 127 (2005) 165–170.
[17] P.V. de Paiva, M. Barbosa, H. Mantelli, L.K. Slongo, Thermal behavior analysis of wire mini heat pipe, J. Heat Transfer 133 (2011) 121502.
[18] S. Launay, V. Sartre, M. Lallemand, Experimental study on silicon micro-heat pipe arrays, Appl. Therm. Eng. 24 (2004) 233–243.
[19] M. Ivanova, A. Lai, C. Gilot, et al., Design, fabrication and test of silicon heat pipes with radial microcapillary grooves, IEEE (2006) 545–551.
[20] J.S. Park, J.H. Choi, H.C. Cho, et al., Flat micro heat pipe arrays for cooling and thermal management at the package level, Proc. SPIE 4408 (2001) 424–429.
[21] K.S. Yang, C.C. Lin, J.C. Shyu, et al., Performance and two-phase flow pattern for micro flat heat pipes, Int. J. Heat Mass Transfe. 77 (2014) 1115–1123.
[22] C. Ding, G. Soni, P. Bozorgi, et al., A flat heat pipe architecture based on nanostructured titania, J. Microelectromech. Syst. 19 (2010) 878–884.
[23] C. Oshman, B. Shi, C. Li, et al., The development of polymer-based flat heat pipes, J. Microelectromech. Syst. 20 (2011) 410–417.
[24] C. Oshman, Q. Li, L.A. Liew, et al., Thermal performance of a flat polymer heat pipe heat spreader under high acceleration, J. Micromech. Microeng. 22 (2012) 045018.
[25] C. Oshman, Q. Li, L.A. Liew, R. Yang, et al., Flat flexible polymer heat pipes, J. Micromech. Microeng. 23 (2013) 1–6.
[26] M. Famouri, G. Carbajal, C. Li, Transient analysis of heat transfer and fluid flow in a polymer-based Micro Flat Heat Pipe with hybrid wicks, Int. J. Heat Mass Transfe. 70 (2014) 545–555.
[27] S.C. Wong, J.H. Liou, C.W. Chang, Evaporation resistance measurement with visualization for sintered copper-powder evaporator in operating flat-plate heat pipes, Int. J. Heat Mass Transfe. 53 (2010) 3792–3798.
[28] S.C. Wong, H.H. Tseng, S.H. Chen, Visualization experiments on the condensation process in heat pipe wicks, Int. J. Heat Mass Transfe. 68 (2014) 625–632.
[29] S. Lips, F. Lefevre, J. Bonjour, Nucleate boiling in a flat grooved heat pipe, Int. J. Therm. Sci. 48 (2009) 1273–1278.
[30] S. Lips, F. Lefevre, J. Bonjour, Combined effects of the filling ratio and the vapour space thickness on the performance of a flat plate heat pipe, Int. J. Heat Mass Transfe. 53 (2010) 694–702.
[31] S. Lips, F. Lefevre, J. Bonjour, Physical mechanisms involved in grooved flat heat pipes: experimental and numerical analyses, Int. J. Therm. Sci. 50 (2011) 1243–1252.
[32] J. Li, D. Wang, G.P. Peterson, Experimental studies on a high performance compact loop heat pipe with a square flat evaporator, Appl. Therm. Eng. 30 (2010) 741–752.
[33] J.P. Holman, Heat Transfer, ninth ed., McGraw-Hill Companies, Inc., New York, 2002.
[34] A.F. Mills, Heat Transfer, second ed., Prentice Hall, Upper Saddle River, 1999.